Supporting Information

Photophysical Characterization and Rate Constants Analysis

UV-visible absorption spectra were acquired from a Hitachi U-3900 spectrophotometer at 298 K. Doped films were prepared by vacuum deposition, and PL quantum yields (PLQYs), transient PL decay characteristics were conducted. PLQYs were determined on a Horiba JY FL-3 spectrometer equipped with a calibrated integrating sphere. Transient PL decay characteristics were recorded on an Edinburgh FLS 1000 spectrometer. Time-resolved transient PL decay measurements were carried out to investigate delayed fluorescence phenomenon of the molecules in doped films (20 wt% 32clCBP, 32clCXT and 32PclCXT in DPEPO). Rate constants of different kinetic processes were calculated following the equations (S1) - (S6) below:

$$k_p = 1/\tau_p \quad \text{S1}$$

$$k_d = 1/\tau_d \quad \text{S2}$$

$$k_r = \Phi_{PF} \times k_p + \Phi_{DF} \times k_d \quad \text{S3}$$

$$k_{nr} = (1-\Phi_{PL}) \times k_r / \Phi_{PL} \quad \text{S4}$$

$$k_{ISC} = k_p - k_{r,s} - k_{nr} \quad \text{S5}$$

$$k_{RISC} = (k_p \times k_d \times \Phi_{DF}) / (k_{ISC} \times \Phi_{PL}) \quad \text{S6}$$

Where k_p, k_d, k_r, k_{nr}, k_{ISC}, k_{RISC} represent the rate constant of prompt fluorescence decay, delayed fluorescence decay, radiation, non-radiation, intersystem crossing and reverse intersystem crossing, respectively; Φ_{PL}, Φ_{PF}, Φ_{DF}, τ_p and τ_d represent total PLQY, quantum yield of the prompt component, quantum yield of the delayed component, lifetimes of the prompt and delayed components, respectively.

Single-Crystal Structure

Single-crystal X-ray data were determined using a Bruker APEX-II CCD X-ray Single Crystal Diffractometer with a (GaK\a) X-ray source, and single crystals were obtained by slow evaporation of CH_2Cl_2/ methanol mixed solvents for 32clCBP (CCDC: 2387339) and CH_2Cl_2/nH mixed solvents for 32clCXT (CCDC:2387345).

Thermal and Electrochemical Characterization

Using a NETZSCH DSC 214, differential scanning calorimetry (DSC) measurements were carried out in a N_2 environment at a heating rate of 10 ˚C·min^{-1}. Using a NETZSCH TG 209F1 Libra, thermogravimetric analyses (TGA) were performed at a heating rate of 10 ˚C min^{-1} in a N_2 environment. On an electrochemical workstation VMP300 (Bio-Logic), cyclic voltammetry was performed. At a scan rate of 100 mV s^{-1}, the oxidation/reduction potentials were measured in dry dichloromethane solutions with 0.1 M TBAPF6 (tetra butylammoniumhexafluorophosphate) as a supporting electrolyte. HOMO = −4.8 − (E_{ox}–$E_{1/2(Ferrocene)}$), LUMO = HOMO + E_g, where E_{ox} represents the onset oxidation potentials, $E_{1/2(Ferrocene)}$ represents the oxidation potential of ferrocene (F_c/F_{c+}), and E_g represent optical bandgap obtained from the absorption onset.

Device Fabrication and Measurement

The ITO substrates were carefully cleaned with 5% decon water, acetone, and isopropyl alcohol in sequence, and then dried. At vacuum pressure lower than 4×10^{-4} Pa, organic materials and metal

layers were deposited sequentially on the ITO substrates. The electroluminescence spectra and current density-voltage-luminance (J-V-L) characteristics were measured using a TOPCON-SR-UL1R and a Keithley 2400 source.

Synthesis

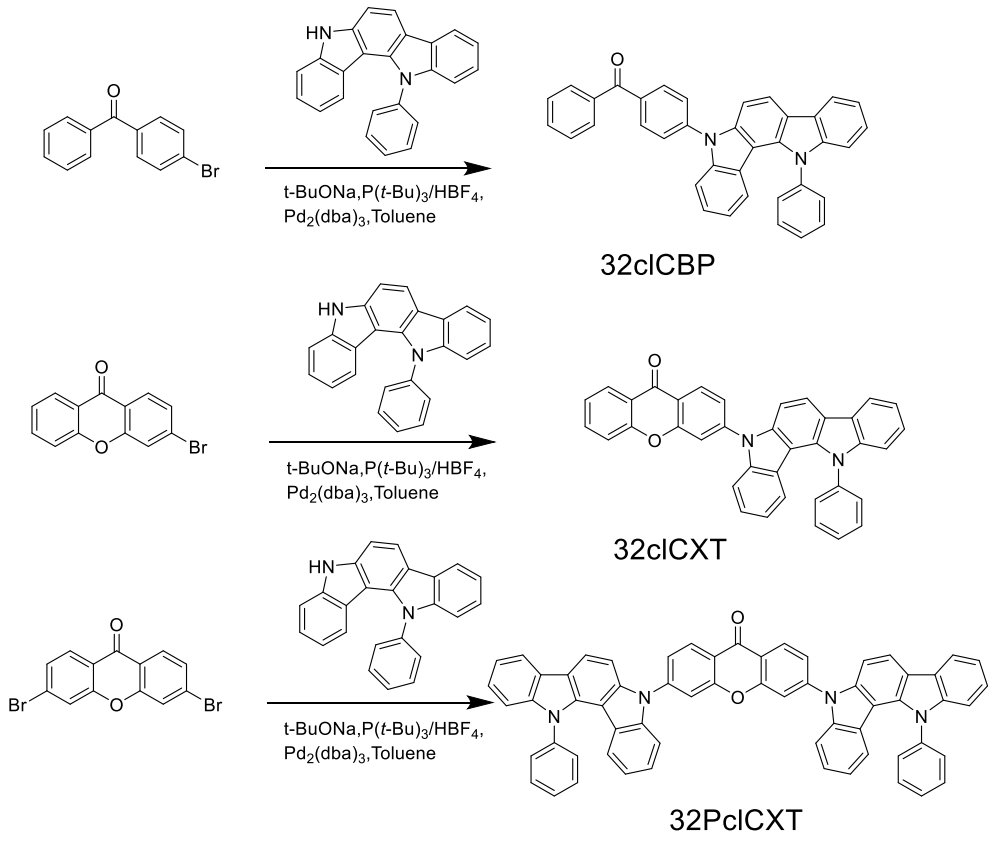

Scheme S1 The synthetic routes of 32clCBP, 32clCXT, 32PclCXT.

32clCBP: To a solution of 4-Bromobenzophenone (0.60 g, 2.3 mmol) in degassed toluene (30 mL), 5,12-Dihydro-12-phenylindolo[3,2-*a*]carbazole (0.84 g, 2.53 mmol), t-BuONa (0.88 g, 9.2 mmol), P(t-Bu)$_3$/HBF$_4$ (0.2g, 0.68 mmol), and Pd$_2$(dba)$_3$ (0.05 g, 0.087 mmol) were added, and the reaction solution was stirred at 120 °C under argon for 10 h. After cooling to room temperature, the mixture was poured into water and extracted with dichloromethane for several times. The combined organic layers were dried over anhydrous sodium sulphate. The mixture was then filtered, and the solvent of the filtrate was removed by rotary evaporation. The crude product was purified by column chromatography on silica gel with n-hexane/dichloromethane (v/v = 2/1) as eluent to get white powder in 50% yield (0.60 g). ^{1}H NMR (600 MHz, Methylene Chloride-d_2) δ 8.23 (d, J = 8.6 Hz, 1H), 8.16 (d, J = 7.0 Hz, 1H), 8.10 (d, J = 8.4 Hz, 2H), 7.93 (d, J = 8.3 Hz, 2H), 7.77 (d, J = 8.4 Hz, 2H), 7.72 – 7.63 (m, 6H), 7.58 (t, J = 7.7 Hz, 2H), 7.44 (dd, J = 21.3, 8.4 Hz, 2H), 7.40 – 7.31 (m,

3H), 7.26 (t, J = 7.6 Hz, 1H), 6.82 (t, J = 7.7 Hz, 1H), 5.98 (d, J = 8.0 Hz, 1H). ^{13}C NMR (151 MHz, CD_2Cl_2) δ 195.37, 142.06, 141.47, 141.10, 140.35, 139.98, 137.48, 136.80, 136.70, 132.61, 131.77, 129.98, 129.95, 129.14, 128.57, 128.43, 127.47, 124.58, 124.44, 124.26, 123.62, 121.78, 120.48, 119.87, 118.90, 118.61, 117.81, 110.19, 109.15, 108.22, 103.51. HR-MS (APCI): m/z calcd for $C_{37}H_{24}N_2O$ $[M+H]^+$ 513.19614, found 513.19634.

32clCXT: The procedure was analogous to that described for 32clC-BP. Green solid of 32clC-XT was obtained in 74% yield (0.71 g). ^{1}H NMR (600 MHz, Methylene Chloride-d_2) δ 8.28 – 8.15 (m, 8H), 7.85 (d, J = 8.3 Hz, 4H), 7.73 – 7.63 (m, 10H), 7.48 (dd, J = 19.7, 8.3 Hz, 4H), 7.41 – 7.27 (m, 8H), 6.83 (t, J = 7.6 Hz, 2H), 6.00 (d, J = 8.1 Hz, 2H). ^{13}C NMR (151 MHz, CD_2Cl_2) δ 194.40, 142.09, 141.74, 141.08, 140.35, 139.98, 136.82, 136.50, 131.84, 129.96, 129.15, 128.59, 127.62, 124.62, 124.47, 124.26, 123.66, 121.84, 120.50, 119.94, 118.92, 118.65, 117.87, 110.21, 109.16, 108.28, 103.51. HR-MS (APCI): m/z calcd for $C_{37}H_{22}N_2O_2$ $[M+H]^+$ 527.17540, found 527.17562.

32PclCXT: The procedure was analogous to that described for 32clC-BP. Green solid of 32PclC-XT was obtained in 74% yield (0.89 g). ^{1}H NMR (600 MHz, Methylene Chloride-d_2) δ 8.63 (d, J = 8.4 Hz, 2H), 8.23 (d, J = 8.6 Hz, 2H), 8.16 (d, J = 7.4 Hz, 2H), 7.86 (s, 2H), 7.75 (d, J = 8.5 Hz, 2H), 7.71 – 7.63 (m, 10H), 7.53 (dd, J = 13.7, 8.5 Hz, 4H), 7.39 – 7.26 (m, 8H), 6.84 (t, J = 7.7 Hz, 2H), 5.99 (d, J = 8.2 Hz, 2H). ^{13}C NMR (151 MHz, CD_2Cl_2) δ 175.40, 157.30, 143.89, 142.14, 140.72, 140.30, 139.68, 136.77, 129.97, 129.12, 128.60, 128.51, 124.78, 124.59, 124.18, 123.74, 123.63, 122.09, 120.94, 120.54, 120.29, 118.98, 118.79, 118.21, 116.51, 110.23, 109.16, 108.55, 103.45. HR-MS (APCI): m/z calcd for $C_{61}H_{36}N_4O_2$ $[M+H]^+$ 857.29110, found 857.29136.

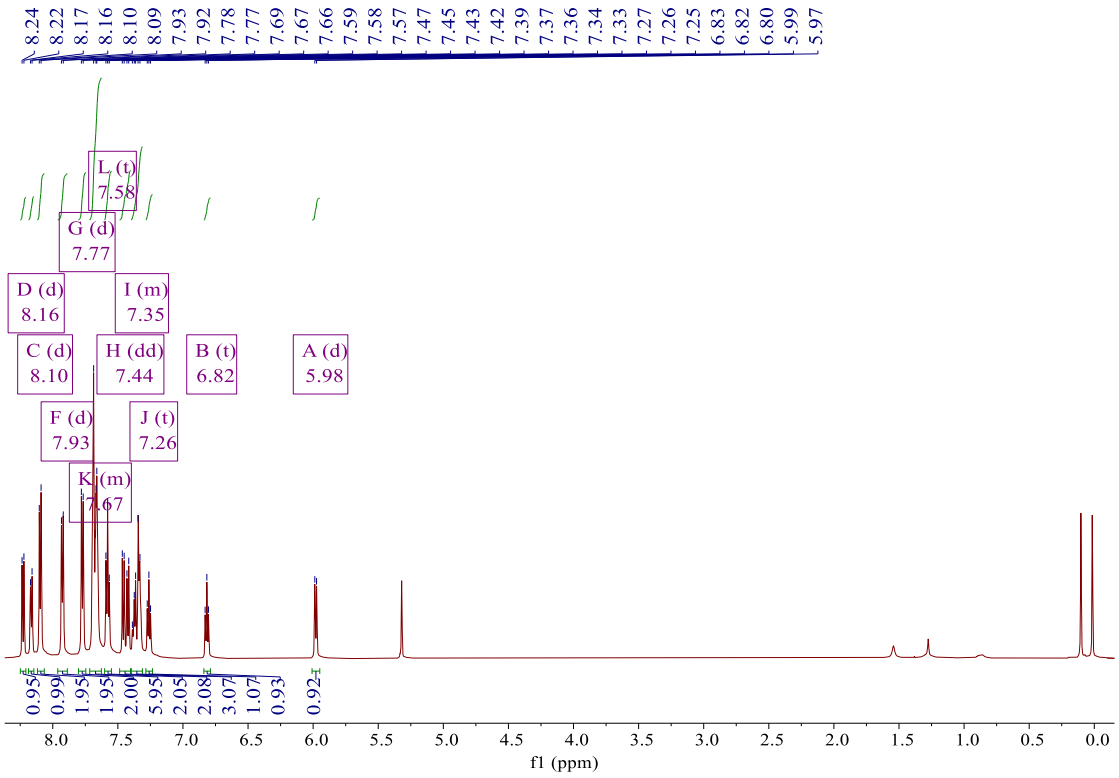

Fig. S1 The ^{1}H NMR of 32clCBP (CD_2Cl_2).

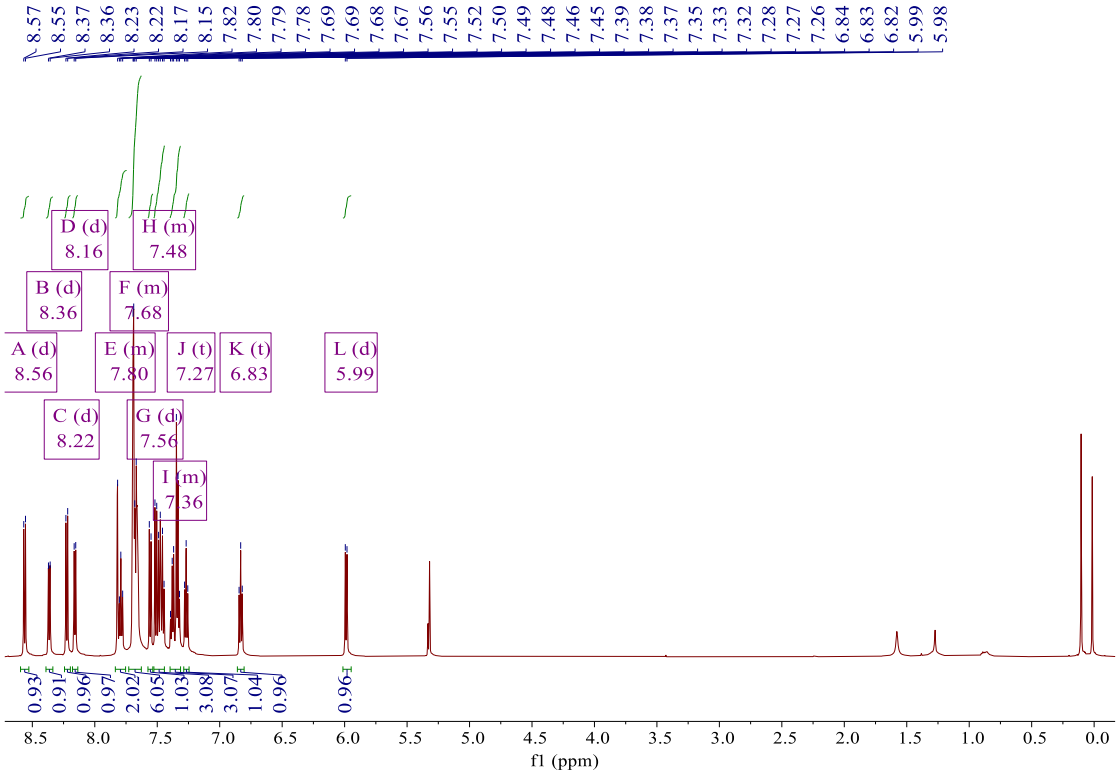

Fig. S2 The ^{1}H NMR of 32clCXT (CD_2Cl_2).

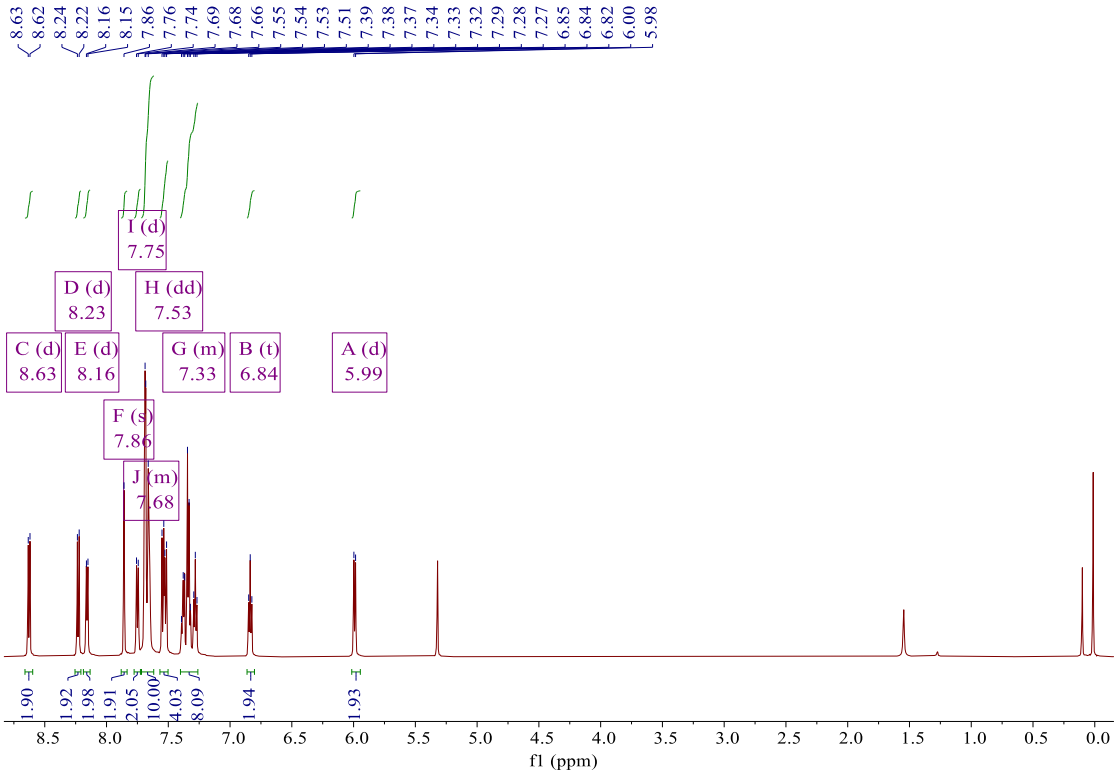

Fig. S3 The ^{1}H NMR of 32PclCXT (CD_2Cl_2).

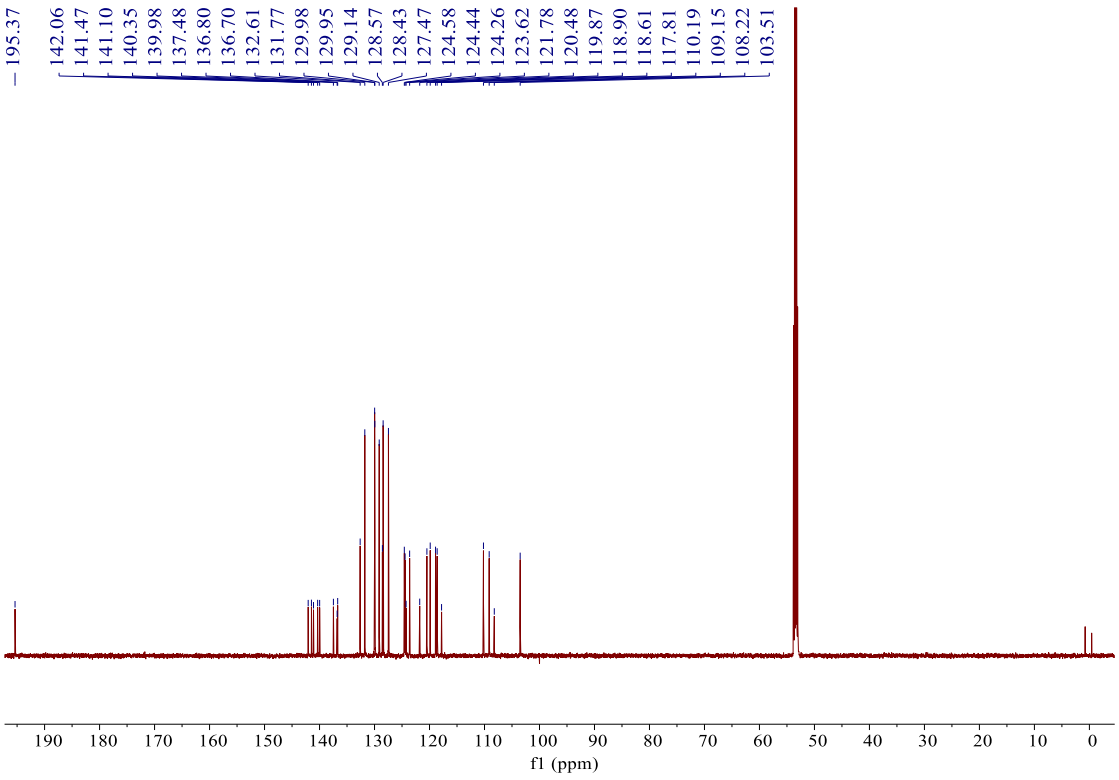

Fig. S4 The ^{13}C NMR of 32clCBP (CD_2Cl_2).

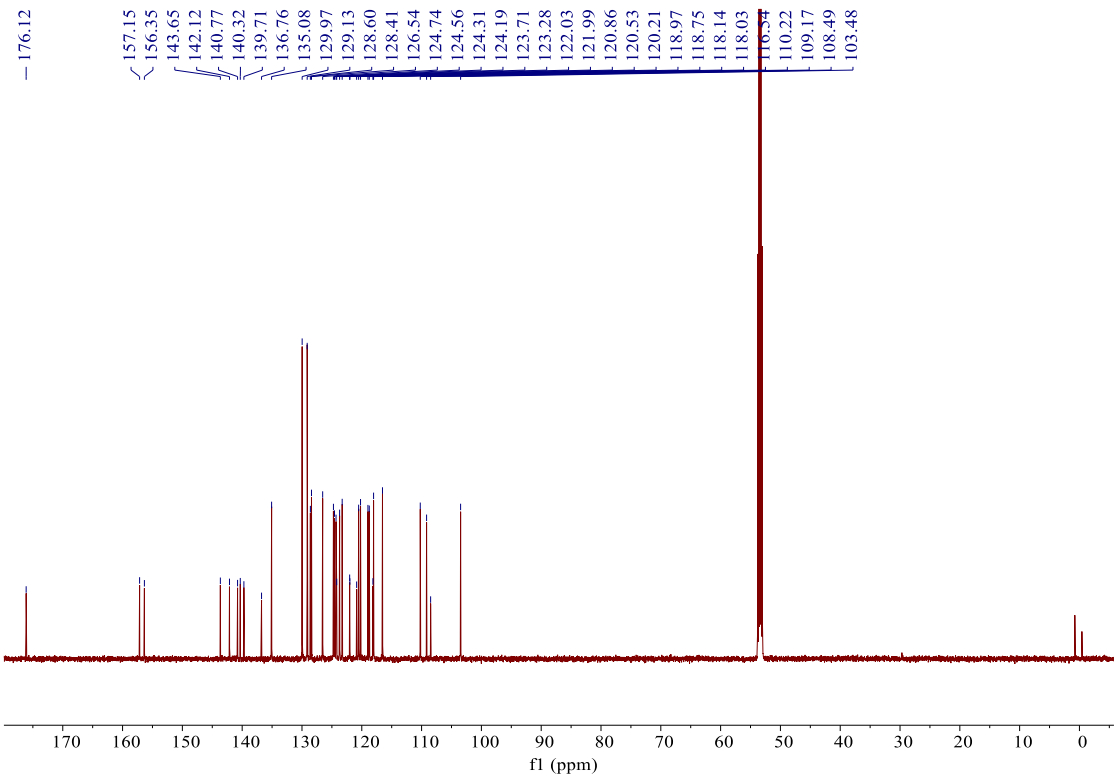

Fig. S5 The ^{13}C NMR of 32clCXT (CD_2Cl_2).

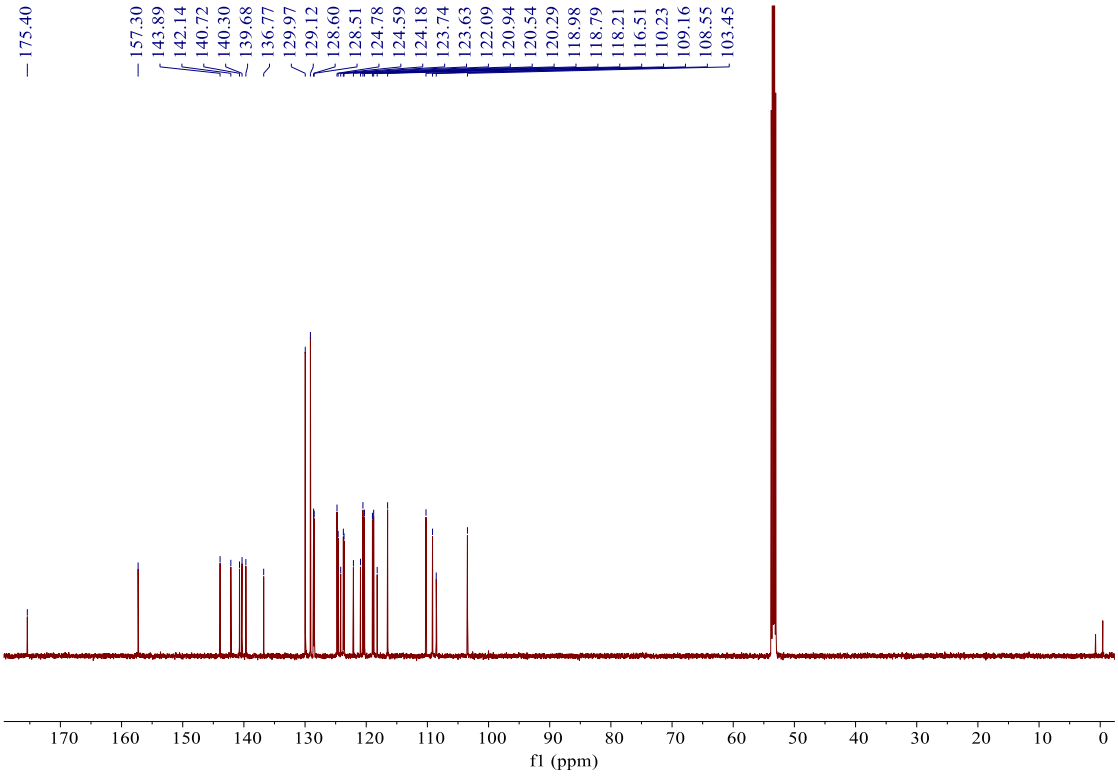

Fig. S6 The ^{13}C NMR of 32PclCXT (CD_2Cl_2).

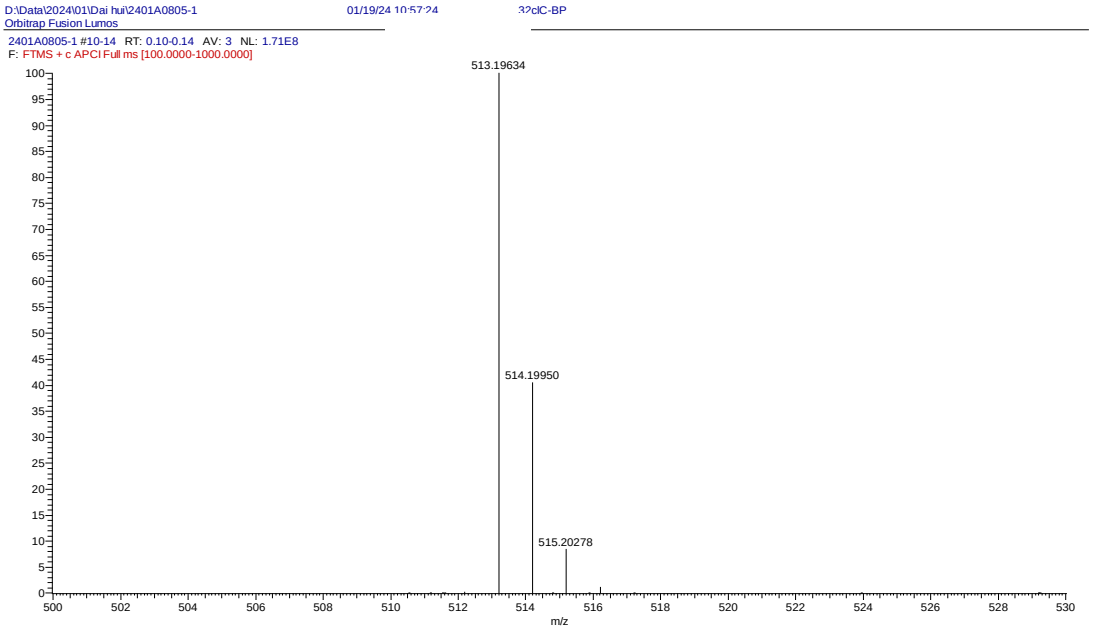

Fig. S7 The HRMS spectrum of 32clCBP.

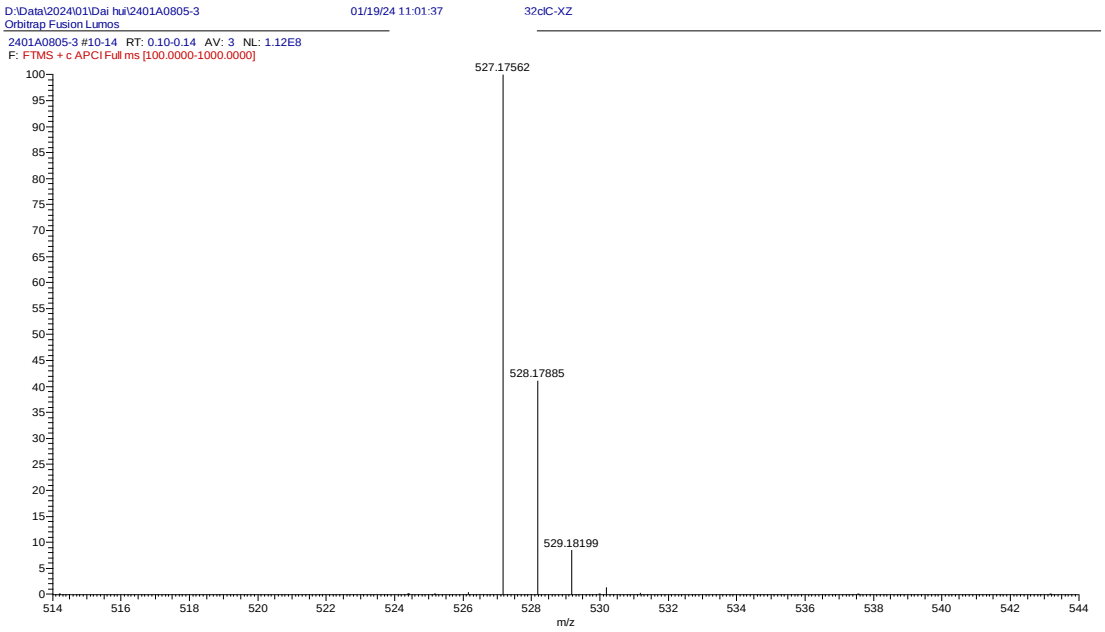

Fig. S8 The HRMS spectrum of 32clCXT.

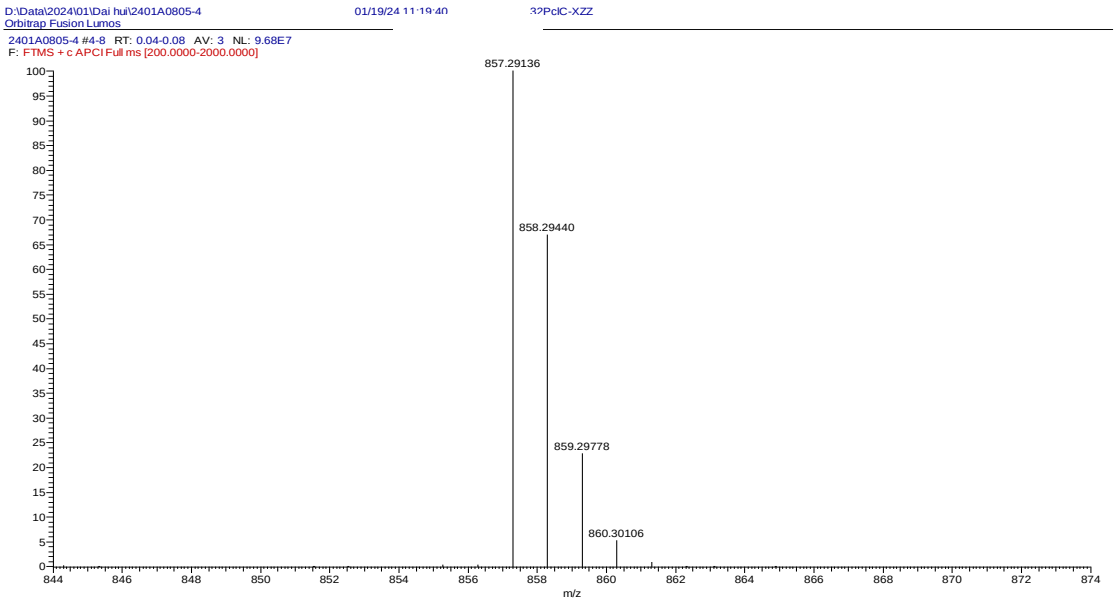

Fig. S9 The HRMS spectrum of 32PclCXT.

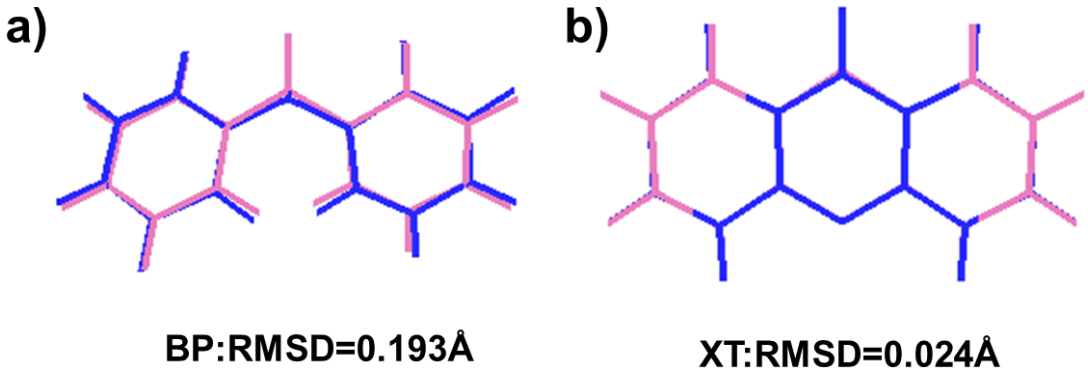

Fig. S10 Geometry comparison between S_0 (pink) and S_1 (blue) states of (a) BP and (b) XT.

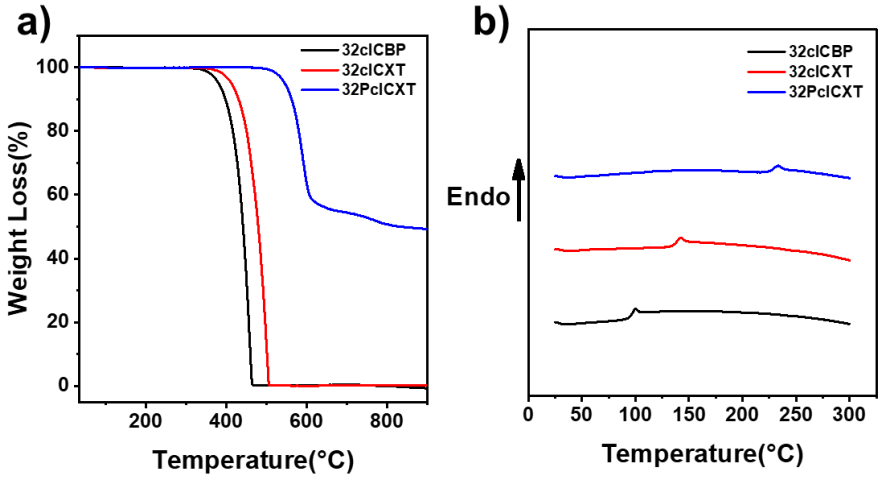

Fig. S11 (a) Thermogravimetric analysis curves, and (b) differential scanning calorimetry curves of 32clCBP, 32clCXT, 32PclCXT.

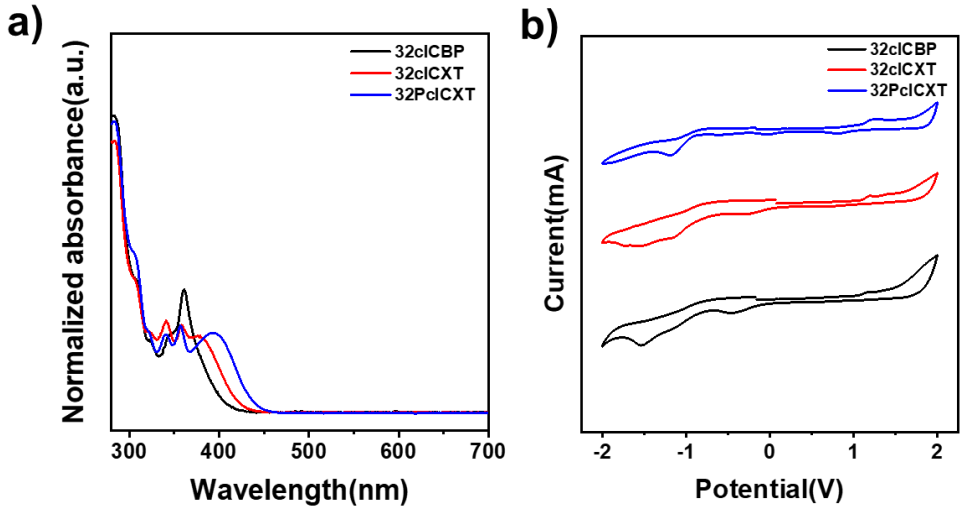

Fig. S12 (a) Ultraviolet-visible absorption spectra of 32clCBP, 32clCXT and 32PclCXT in DCM solutions. (b) Cyclic voltammetry measurements of 32clCBP, 32clCXT and 32PclCXT.

Table S1 Electrochemical parameters of 32clCBP, 32clCXT and 32PclCXT.

Molecule	HOMO (eV)	LUMO (eV)	E_g (eV)
32clCBP	-5.36	-2.43	2.93
32clCXT	-5.39	-2.53	2.86
32PclCXT	-5.38	-2.63	2.75

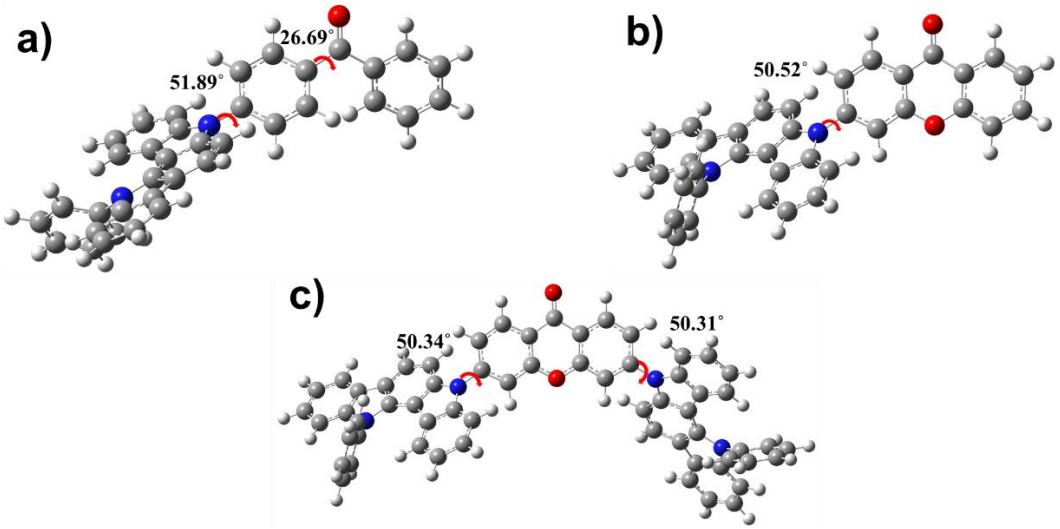

Fig. S13 Calculated dihedral angles in (a) 32clCBP, (b) 32clCXT, and (c) 32PclCXT from their optimized structures in S_0 state.

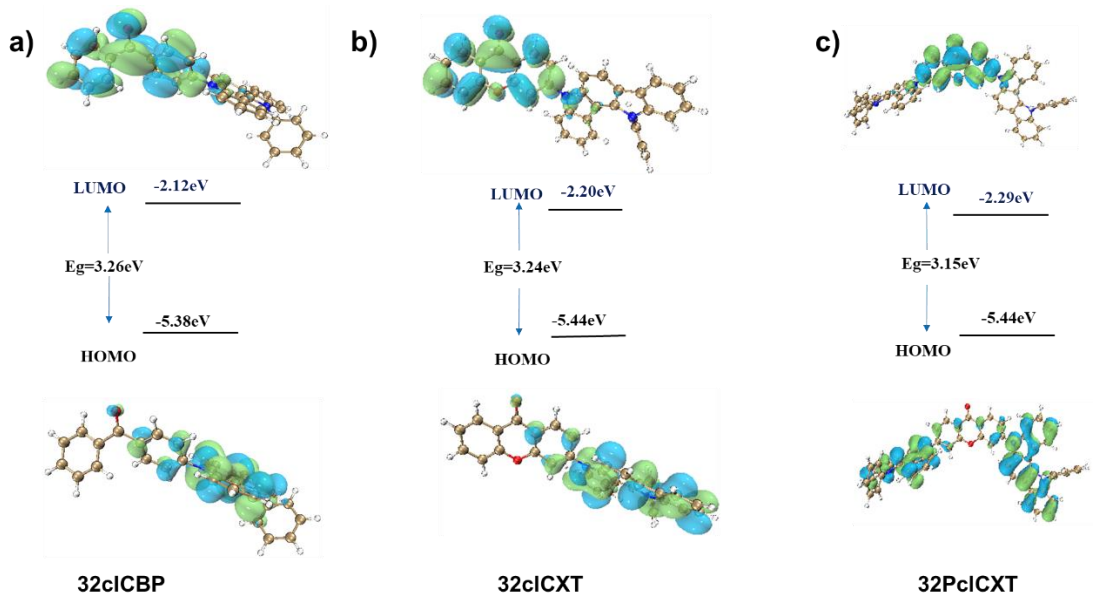

Fig. S14 Spatial HOMO and LUMO distributions of 32clCBP, 32clCXT and 32PclCXT.

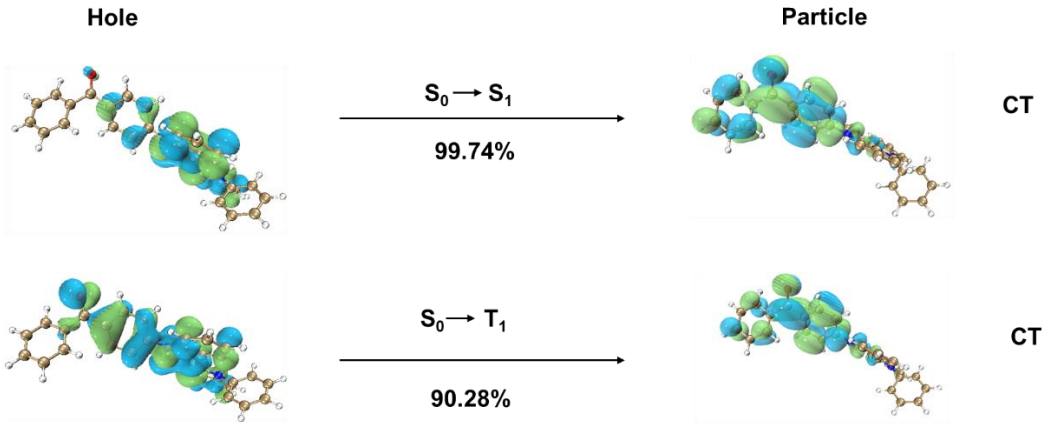

Fig. S15 The NTO analysis of S_1 and T_1 states for 32clCBP.

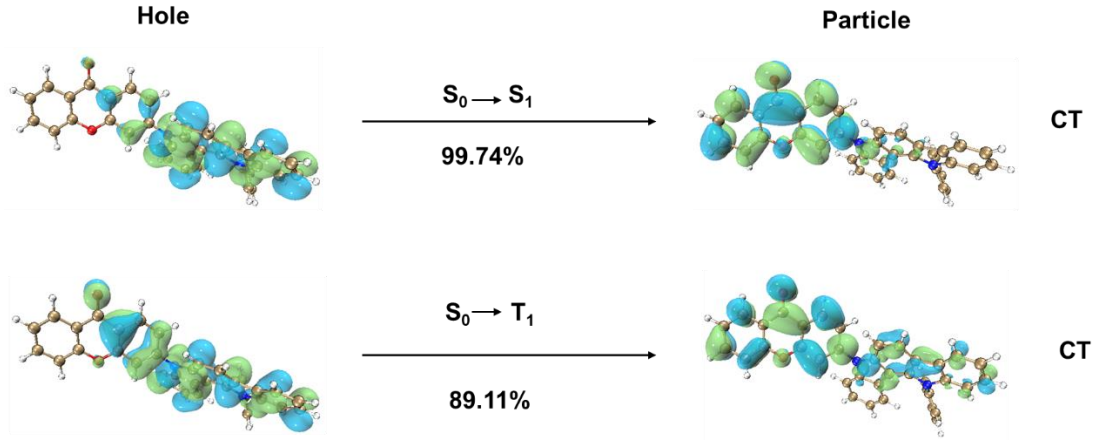

Fig. S16 The NTO analysis of S_1 and T_1 states for 32clCXT.

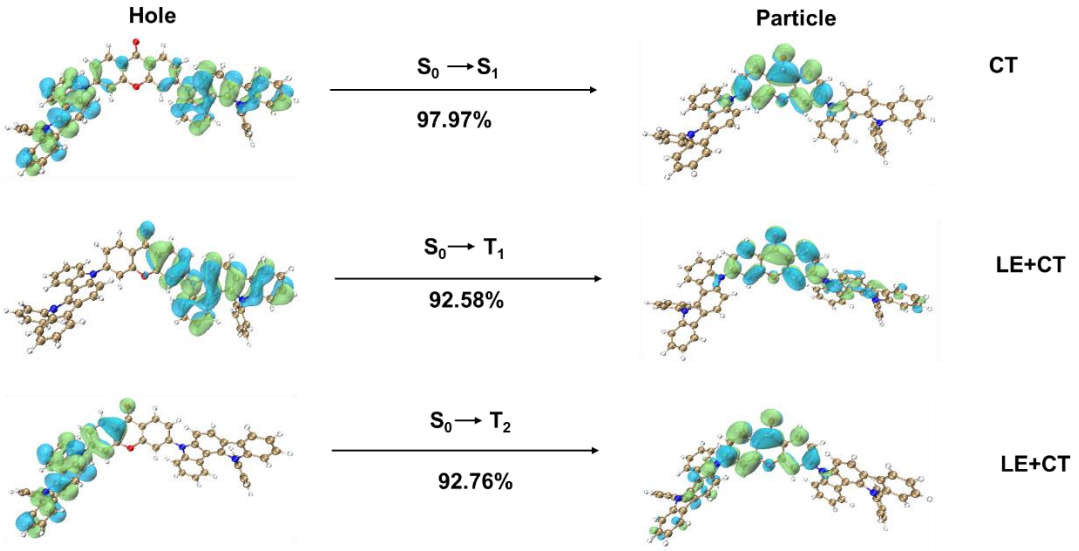

Fig. S17 The NTO analysis of S_1 and T_1 states for 32PclCXT.

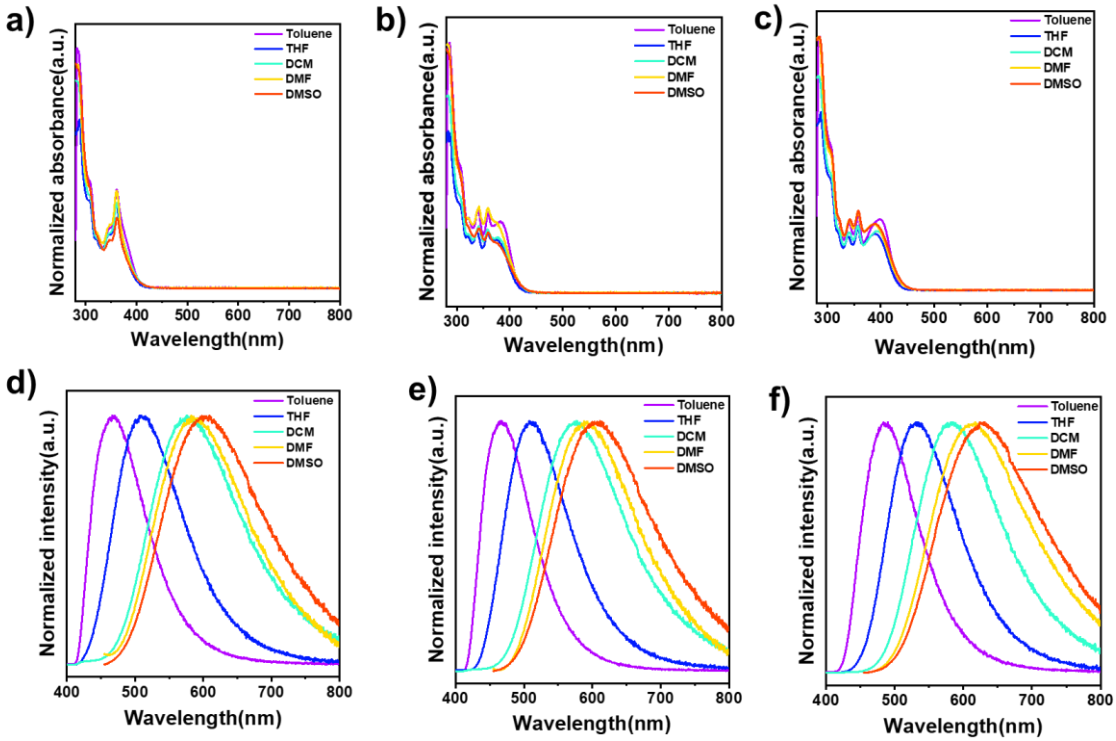

Fig. S18 Ultraviolet-visible absorption spectra of (a) 32clCBP, (b) 32clCXT, (c) 32PclCXT and PL spectra of (d) 32clCBP, (e) 32clCXT, (f) 32PclCXT in different solutions.

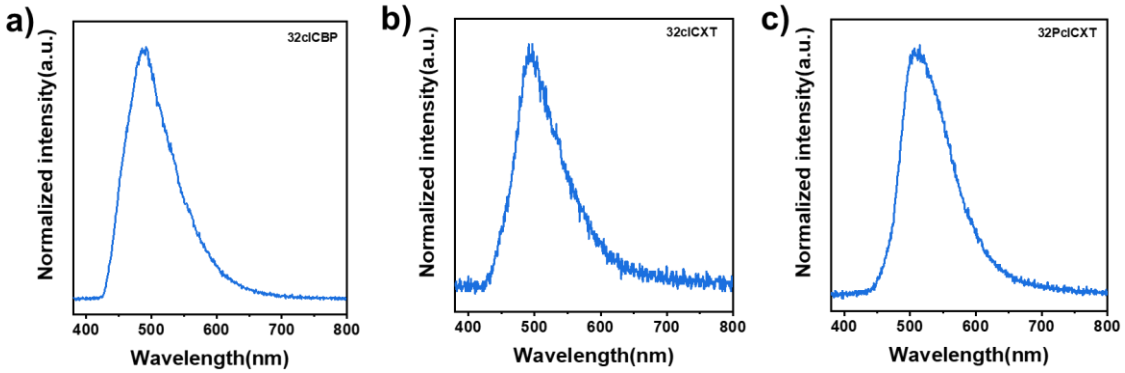

Fig. S19 Phosphorescence spectra of (a) 32clCBP, (b) 32clCXT and (c) 32PclCXT in DMSO solutions at 77 K.

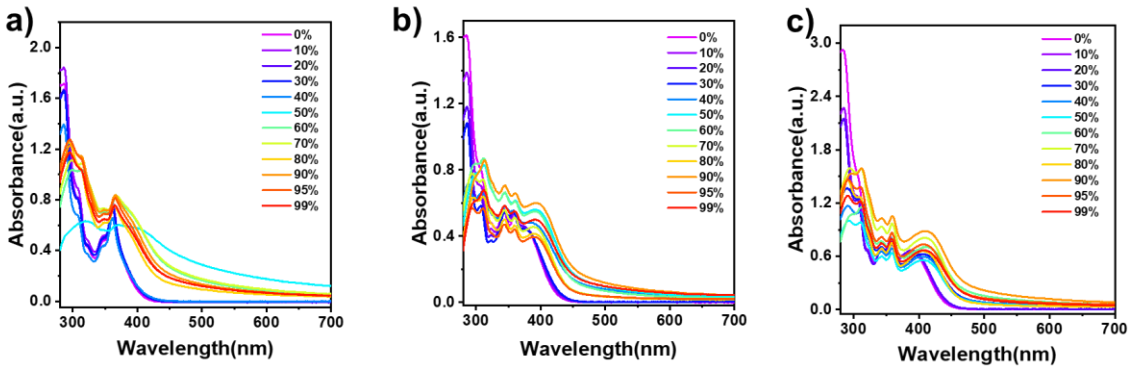

Fig. S20 Ultraviolet-visible absorption spectra of (a) 32clCBP, (b) 32clCXT, and (c) 32PclCXT in H_2O/DMSO mixtures with different water contents.

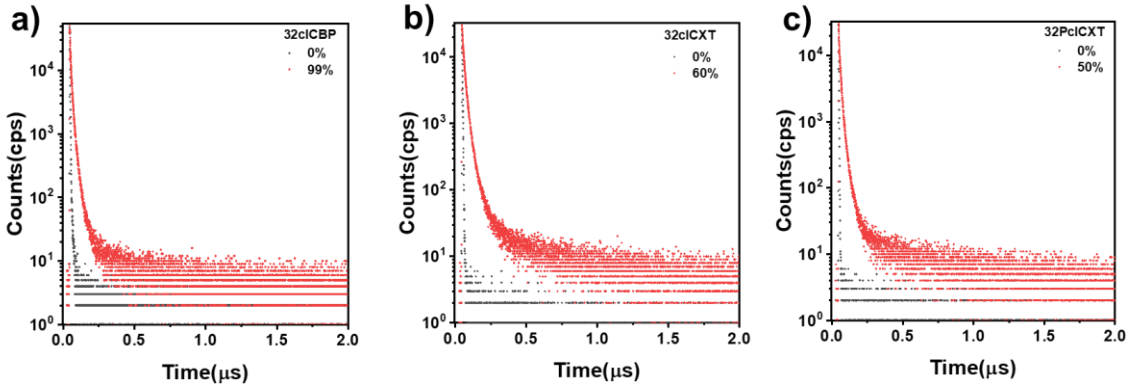

Fig. S21 The transient PL decays of (a) 32clCBP, (b) 32clCXT, and (c) 32PclCXT in DMSO/H_2O mixtures.

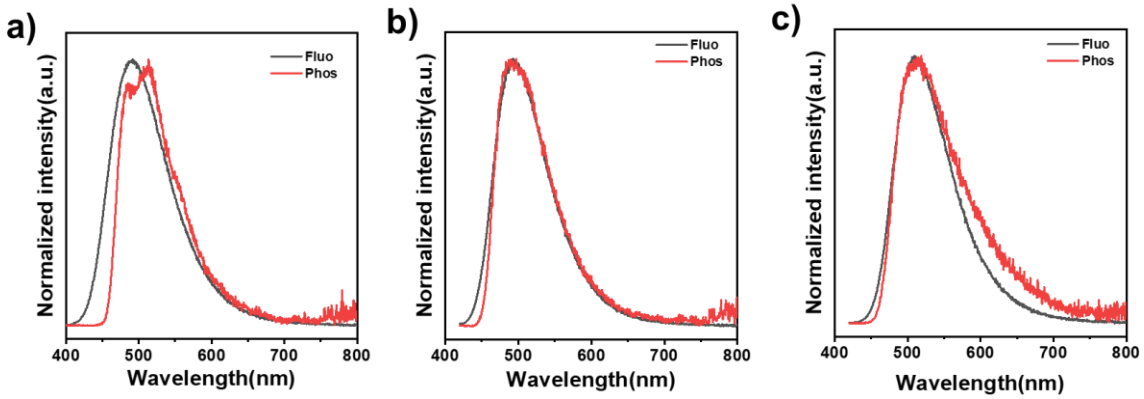

Fig. S22 Room-temperature fluorescence and phosphorescence spectra at 77 K of (a) 32clCBP, (b) 32clCXT and (c) 32PclCXT in doped films.

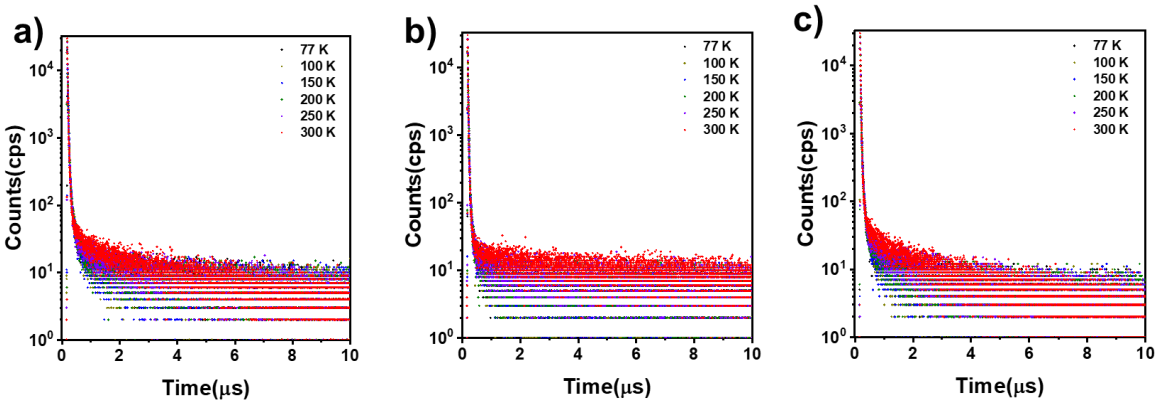

Fig. S23 Temperature-dependent transient PL decay spectra of (a) 32clCBP, (b) 32clCXT, and (c) 32PclCXT doped in DPEPO host with a doping concentration of 20 wt%, measured under nitrogen.

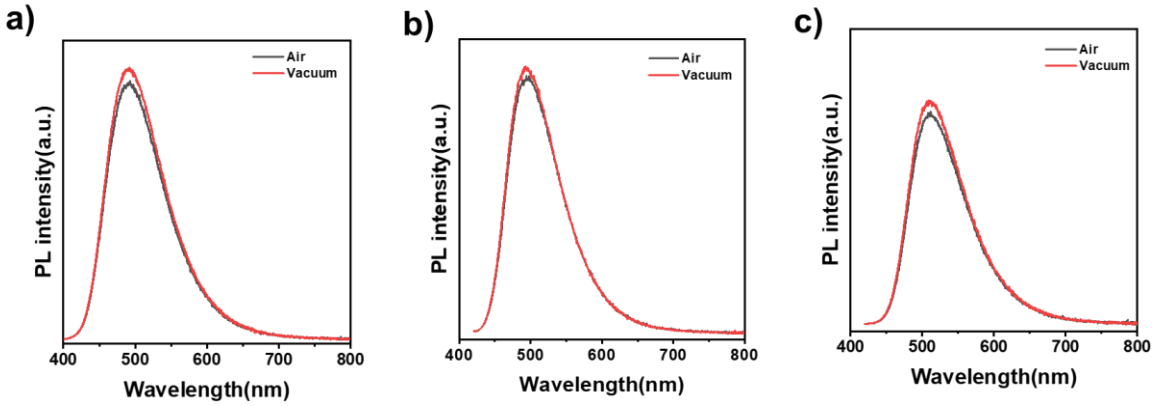

Fig. S24 PL spectra of (a) 32clCBP, (b) 32clCXT and (c) 32PclCXT in doped films under air and vacuum.

Table S2 Crystal data and structure refinement for the two single crystals.

Compound	**32clCBP**	**32clCXT**
formula	$C_{37}H_{24}N_2O$	$C_{37}H_{22}N_2O_2$
fw	512.58	526.56
crystal system	triclinic	triclinic
T/K	150.0	149.99(10)
space group	P-1	P-1
a/Å	6.499(3)	5.7116(5)
b/Å	11.218(4)	12.3669(9)
c/Å	17.798(8)	18.6670(14)
α/°	97.448(14)	102.633(6)
β/°	93.423(14)	91.040(6)
γ/°	90.73(2)	92.503(6)
Volume/Å^3, Z	1284.1(9), 2	1284.87(18), 2
ρ_{calc}g/cm^3	1.326	1.361
μ/mm^{-1}	0.396	0.085
F(000)	536.0	548.0
Crystal size/mm^3	0.3 × 0.008 × 0.005	0.18 × 0.12 × 0.08
Radiation	Ga Kα (λ = 1.34138)	Mo Kα (λ = 0.71073)
2Θ range for data collection/°	4.36 to 119.56	4.98 to 65.892
Index ranges	-8 ⩽ h ⩽ 8, -14 ⩽ k ⩽ 13, -22 ⩽ l ⩽ 22	-8 ⩽ h ⩽ 8, -18 ⩽ k ⩽ 18, -27 ⩽ l ⩽ 26
Reflections collected	17318	14566
Independent reflections	5672 [R_{int} = 0.0733, R_{sigma} = 0.0830]	8535 [R_{int} = 0.0433, R_{sigma} = 0.0990]
Data/restraints/parameters	5672/0/362	8535/0/370
Goodness-of-fit on F^2	1.019	0.991
Final R indexes [I>=2σ (I)]	R_1 = 0.0614, wR_2 = 0.1470	R_1 = 0.0737, wR_2 = 0.1544
Final R indexes [all data]	R_1 = 0.1119, wR_2 = 0.1763	R_1 = 0.1437, wR_2 = 0.1950
Largest diff. peak/hole / e Å^{-3}	0.31/-0.31	0.36/-0.32

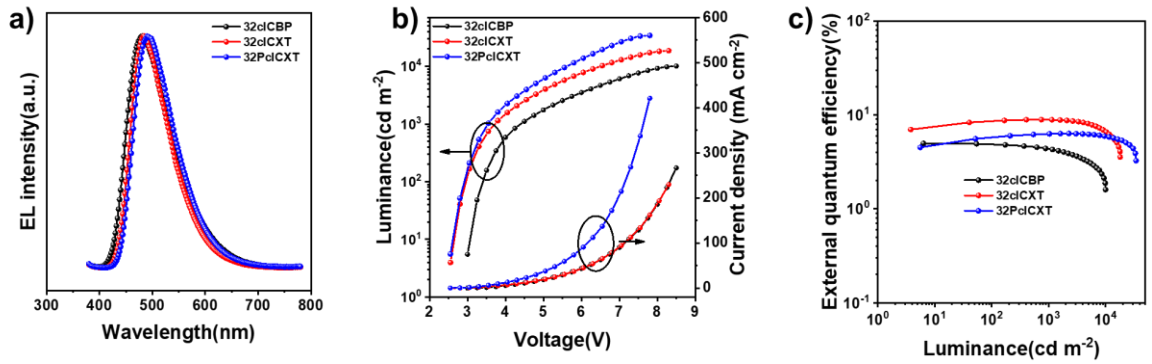

Fig. S25 (a) EL spectra, (b) luminance–voltage–current density, and (c) external quantum efficiency–luminance curves of non-doped OLEDs based on 32clCBP, 32clCXT and 32PclCXT.

Table S3 EL performances of the non-doped OLEDs based on 32clCBP, 32clCXT and 32PclCXT.

EML	λ_{EL} [nm]	V_{on} [V]	L_{max} [cd/m^2]	CE_{max} [cd/A]	PE_{max} [Im/W]	EQE_{max} [%]
32clCBP	481	3.0	10002	11.9	12.5	5.0
32clCXT	484	2.5	18700	22.3	22.7	8.9
32PclCXT	491	2.5	34226	17.4	17.3	6.3

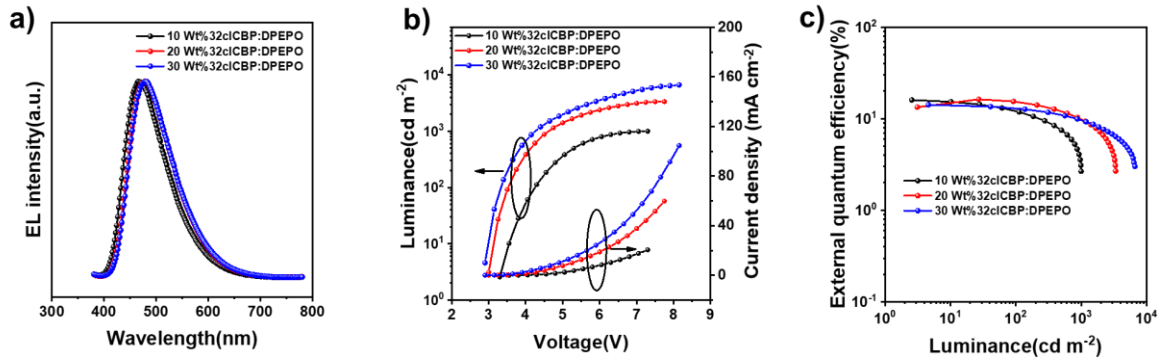

Fig. S26 (a) EL spectra, (b) luminance–voltage–current density, and (c) external quantum efficiency–luminance curves of doped OLEDs based on 32clCBP with different doping concentrations.

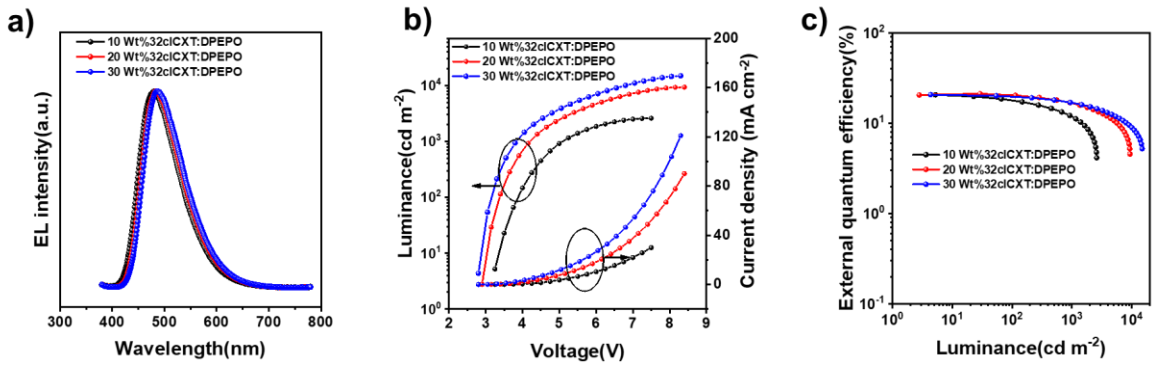

Fig. S27 (a) EL spectra, (b) luminance–voltage–current density, and (c) external quantum efficiency–luminance curves of doped OLEDs based on 32clCXT with different doping concentrations.

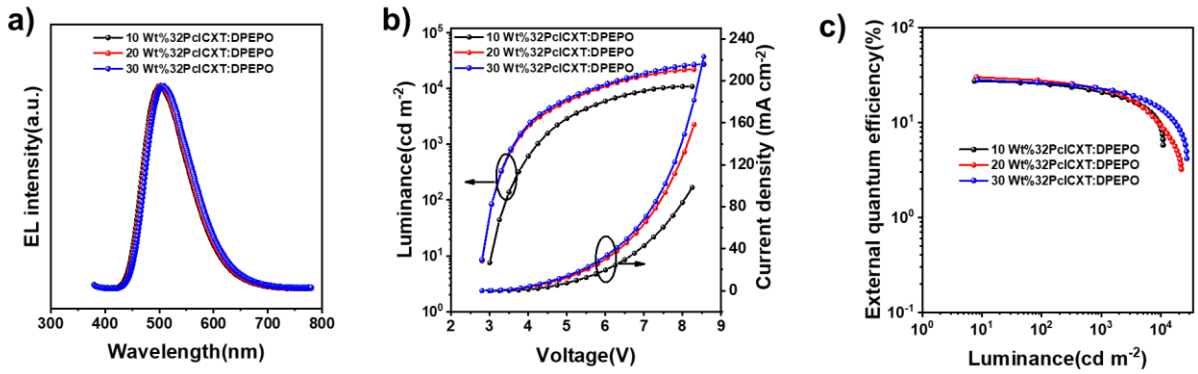

Fig. S28 (a) EL spectra, (b) luminance–voltage–current density, and (c) external quantum efficiency–luminance curves of doped OLEDs based on 32PclCXT with different doping concentrations.

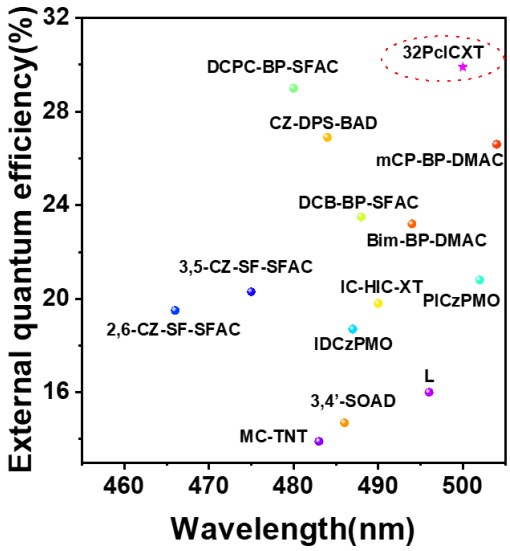

Fig. S29 EQE summary of TADF materials with EL spectral peaks between 465-505 nm.

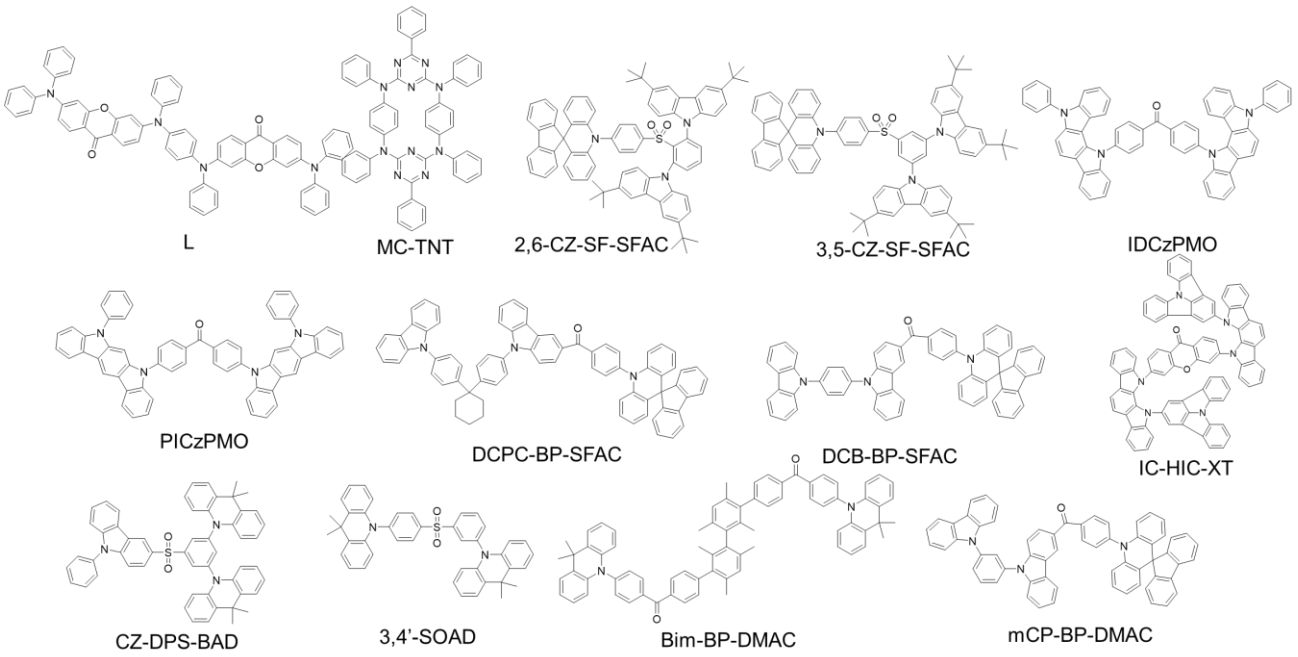

Fig. S30 Chemical structures of reported molecules listed in Fig. S29.

Table S4 Detailed EL performance summary of TADF materials listed in Fig. S29.

Compound	EL [nm]	EQE_{max} [%]	Ref.
32PclCXT	500	29.9	This Work
L	496	16	1
MC-TNT	483	13.9	2
2,6-CZ-SF-SFAC	466	19.5	3
3,5-CZ-SF-SFAC	475	20.3	3
IDCzPMO	487	18.7	4
PICzPMO	502	20.8	4
DCPC-BP-SFAC	480	29.0	5
DCB-BP-SFAC	488	23.5	6
IC-HIC-XT	490	19.8	7
CZ-DPS-BAD	516	21.5	8
3,4'-SOAD	486	14.7	9
Bim-BP-DMAC	494	23.2	10
mCP-BP-DMAC	504	26.6	11

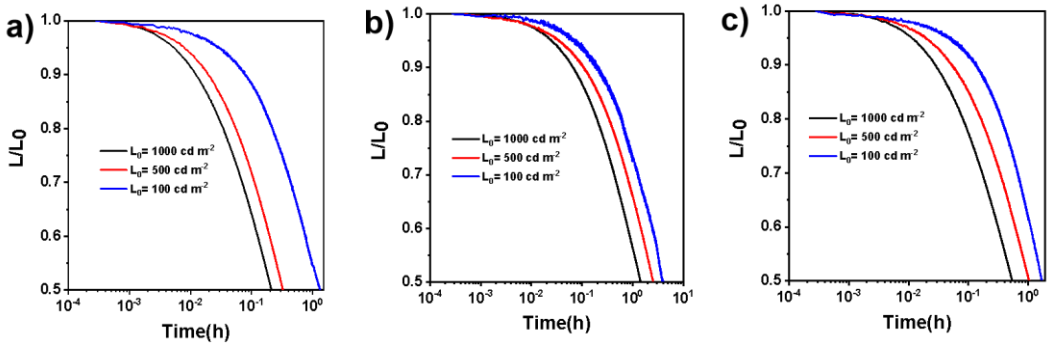

Fig. S31 Operational lifetimes of the 20 wt % doped devices based on (a) 32clCBP, (b) 32clCXT, and (c) 32PclCXT.

References

1. Y. Fu, Z. Ye, D. Liu, Y. Mu, J. Xiao, D. Hu, S. Ji, Y. Huo and S.-J. Su, *Adv. Mater.*, 2023, **35**, 2301929.
2. J. Xiao, D. Liu, Y. Fu, W. Xie, Y. Mu, J.-X. Chen, Z. Ye, S. Ji, Y. Huo and S.-J. Su, *Angew. Chem. Int. Ed.*, 2024, e202415680.
3. J. Zhang, D. Li, W. Li, Y. Meng and Z. Ge, *Laser Photonics Rev.*, 2024, **18**, 2300758.
4. J. Wang, Y. Yang, F. Gu, X. Zhai, C. Yao, J. Zhang, C. Jiang and X. Xi, *ACS Appl. Mater. Interfaces*, 2023, **15**, 59643–59654.
5. Y. Fu, H. Liu, D. Yang, D. Ma, Z. Zhao and B. Z. Tang, *Adv. Opt. Mater.*, 2022, **10**, 2102339.
6. H. Chen, H. Liu, P. Shen, J. Zeng, R. Jiang, Y. Fu, Z. Zhao and B. Z. Tang, *Adv. Opt. Mater.*, 2021, **9**, 2002019.
7. X. Lan, J. Zeng, J. Chen, T. Yang, X. Dong, B. Z. Tang and Z. Zhao, *Angew. Chem. Int. Ed.*, 2024, e202414488.
8. J. Huo, S. Xiao, Y. Wu, M. Li, H. Tong, H. Shi, D. Ma and B. Z. Tang, *Chem. Eng. J.*, 2023, **452**, 138957.
9. J. Li, Y. Xia, G. Li, M. Chen, J. Zhou, W. Yan, B. Zhao, K. Guo and H. Wang, *Chem. Eng. J.*, 2023, **470**, 143966.
10. X.-L. Chen, X.-D. Tao, Z. Wei, L. Meng, F.-L. Lin, D.-H. Zhang, Y.-Y. Jing and C.-Z. Lu, *ACS Appl. Mater. Interfaces*, 2021, **13**, 46909-46918.
11. X. Wu, J. Zeng, X. Peng, H. Liu, B. Z. Tang and Z. Zhao, *Chem. Eng. J.*, 2023, **451**, 138919.